JOURNAL OF AIRCRAFT
Vol. 33, No. 5, September–October 1996

# Fatigue Life of Panels with Multiple Site Damage

E. J. Moukawsher*
*U.S. Coast Guard Repair and Supply Center, Elizabeth City, North Carolina 27909*
and
A. F. Grandt Jr.† and M. A. Neussl‡
*Purdue University, West Lafayette, Indiana 47907-1282*

**This article describes research aimed at predicting the fatigue lives of unstiffened aluminum panels that contain multiple site damage (MSD). The initial damage consists of through-the-thickness cracks emanating from a row of holes in the center of a finite width panel. The row of holes is aligned perpendicular to a cyclically applied, constant amplitude, tensile load. A fracture mechanics analysis is employed to predict the growth, interaction, and coalescence of the various cracks that propagate in the panel. A strain-life analysis incorporating Neuber's rule for notches, and Miner's rule for cumulative damage, is also employed to predict crack initiation for holes with no initial cracking. Twelve fatigue tests of 2024-T3 aluminum panels with MSD were conducted to evaluate the analysis, and the test results compare favorably with predictions for the fatigue life of these panels. Crack interaction effects in the MSD test specimens are apparent, and are shown to significantly accelerate crack growth rates, particularly during the latter stages of fatigue life.**

## Introduction

MULTIPLE SITE DAMAGE (MSD) refers to the existence of simultaneous fatigue cracking at various structural locations, and has occurred along rows of fastener holes in the fuselages and wings of commercial and military aircraft. MSD is significant when it reduces the overall structural integrity more than would be predicted by the analysis of individual cracks, or when the cracks are close enough together to influence each other's growth rates.[1,2] Significant MSD cracking may develop before it can be reliably detected by many nondestructive evaluation (NDE) techniques. MSD may also reduce the residual strength (RS) of panels below that predicted by simple analytical techniques. (For the purposes of this investigation, RS is defined as the maximum stress a panel can sustain before complete failure occurs across the center span.)

MSD poses a significant challenge to those who must ensure the structural integrity of aging aircraft because it is extremely difficult to detect, greatly reduces the RS and critical crack size, and may defeat the crack arrest capability of the design.[3,4] The most widely known failure attributed to MSD is the Aloha Airlines incident of April 28, 1988, in which a 4.5-m- (15-ft-) long section of fuselage structure was peeled-open in flight, resulting in the death of a flight attendant and the near-loss of the entire aircraft.[5]

The objective of this article is to describe a procedure for predicting the fatigue crack growth properties and interaction effects of MSD cracks through the study of a simplified MSD scenario. The approach focuses on predicting the fatigue lives and individual crack growth at open fastener holes in flat, unreinforced panels subjected to cyclic, constant amplitude loads. The effect of MSD on the RS of these panels is described in a companion article,[6] and additional details of the analysis and experiments are given in Ref. 7.

Received Sept. 27, 1995; revision received Feb. 15, 1996; accepted for publication May 15, 1996. 

*Chief of Aeronautical Engineering. (Deceased).
†Professor, School of Aeronautics and Astronautics, 1282 Grissom Hall. Associate Fellow AIAA.
‡Graduate Student; currently Engineering Officer, U.S. Coast Guard Air Station, 2185 SE 12th Place, Warrenton, OR 97146.

## Experimental Procedures

A testing program was conducted to evaluate the accuracy of a numerical method for predicting the fatigue life of panels with MSD. To accomplish this goal, fatigue testing was conducted to investigate fatigue crack initiation, crack growth, and crack interaction effects in panels that contain MSD. The test material was 2.3-mm- (0.09-in.-) thick 2024-T3 aluminum (bare), procured commercially in two separate lots consisting of four 1.2 × 3.7 m (4 × 12 ft) sheets. Specimens were oriented so that the grain direction was perpendicular to the loading axis. A typical MSD specimen is shown in Fig. 1.

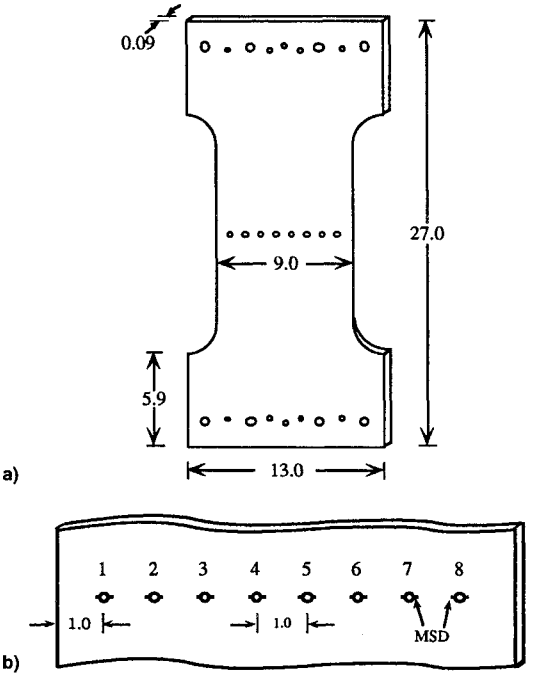


**Fig. 1 Typical MSD specimen (MSD04) with nominal 0.16-in. hole diameter: a) global specimen configuration (dimensions in inches) and b) detailed view of crack plane showing hole spacing and MSD crack locations (dimensions in inches).**

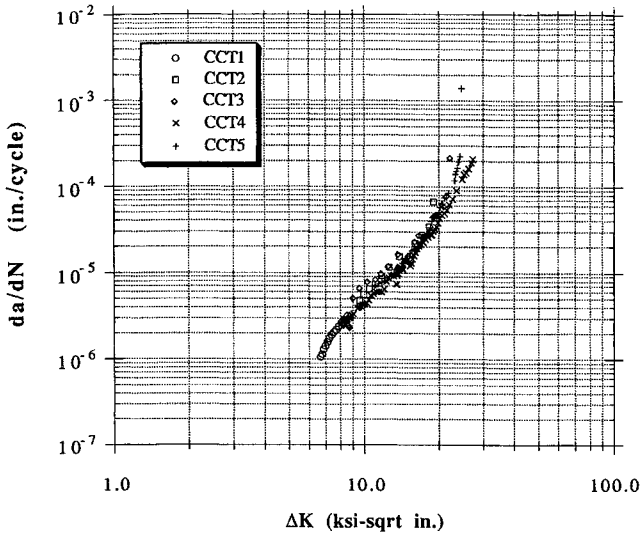


**Fig. 2 Fatigue crack growth rate data for 2024-T3 aluminum test material.**

### Baseline Testing

An MTS test machine was used to measure the tensile ultimate $\sigma_u$ and yield $\sigma_{ys}$ stresses in rectangular specimens according to ASTM specification E-8.[8] An extensometer was used to measure the strain across a 1-in. span under load control. The 0.2% offset yield stress $\sigma_{ys}$ was determined to be 303 MPa (44.0 ksi) and the ultimate stress $\sigma_u$ was found to be 434 MPa (63 ksi).

Fatigue crack growth tests were conducted in accordance with ASTM Standard E-647[9] to determine the basic fatigue crack growth rate $da/dN$ vs the cyclic stress intensity factor $\Delta K$ relationship for the 2024-T3 test material. Five center crack tension (CCT) specimens were milled from the test panels using a Flow International Corporation Abrasive Jet Cutting System (model 430). Constant amplitude, uniaxial, $R$ = 0.01 loading at a frequency of 5 Hz was applied parallel to the specimen's major axis until failure occurred. The crack growth data were reduced according to the seven-point polynomial approach described in Ref. 9, and are given in the form of a $da/dN - \Delta K$ plot in Fig. 2. The nine points from these data given in Table 1 were used to define a set of segmented Paris laws for subsequent life predictions.

### MSD Fatigue Tests

Twelve fatigue tests of 22.9-cm- (9-in.-) wide specimens shown schematically in Fig. 1 were conducted to determine the fatigue lives of panels with MSD, and to measure the growth of interacting cracks in MSD configurations. Two types of MSD panels with nominal hole diameters of 4.06 mm (0.16 in.) were tested. The two types, designated type A and type B, had the same overall design shown in Fig. 1, differing only in their hole and crack configurations. Type A specimens contained small, nearly uniform MSD cracks at all holes. Type A panels with eight holes spaced 2.5 cm (1.0 in.) apart and with 10 and 11 holes spaced 1.9 cm (0.75 in.) apart were tested. Figure 3 shows the hole and crack configuration for the type A panels.

The type B panels had relatively large lead cracks that spanned several of the central holes. Type B panels with MSD at all holes and with MSD at only some of the holes were tested. One type B panel with no holes precracked was also tested to demonstrate the reduction of fatigue life caused by MSD. Figures 4 and 5 depict the designs of the type B panels.

The MSD specimen preparation followed the following procedures. First, the sheets of 2.3-mm- (0.09-in.-) thick 2024-T3 aluminum were sheared to a length of 69 cm (27 in.) and a width of 33 cm (13 in.). These sheets were flattened with a mechanical roller to remove warping present in the original 1.2 × 3.7 m (4 × 12 ft) sheet. Next, a 20-cm- (8-in.-) wide section was polished to a mirror-like finish across the center span of one side to aid in viewing the cracks with an optical microscope. The sheet was then milled to the final specimen dimensions using the abrasive jet machining tool described previously. Small fatigue starter-notches (1 mm = 0.04 in. long by 0.25 mm = 0.01 in. wide) were cut at both sides of MSD holes with the abrasive jet tool. Although rounded at the ends (with a radius of approximately 0.13 mm = 0.005 in.), these slots produced early and consistent crack initiation during fatigue precracking.

Each specimen was precracked under constant amplitude cyclic loading until measurable cracks were visible under the optical microscope at both sides of all holes with starter notches. The type B MSD specimens were initially cycled at double their test loading to reduce the total time to crack initiation. Loads were then reduced in increments of 20% or less as prescribed by ASTM Standard E647[9] until measurable crack growth at the final test load was achieved. Only the type B specimens required this load shedding procedure, as the precracking load used on the type A specimens was the same as the test load. The central ligament between the holes forming the lead crack in the type B specimens was cut with a jeweler's saw after the holes were fatigue precracked. This procedure

**Table 1 Points used to define the Paris law segments for the fatigue crack growth behavior of the 2024-T3 aluminum test material**

| $\Delta K$, ksi-$\sqrt{\text{in.}}$ | $da/dN$, in./cycle |
|---|---|
| 3.65 | $2.40 \times 10^{-7}$ |
| 6.68 | $1.07 \times 10^{-6}$ |
| 7.11 | $1.58 \times 10^{-6}$ |
| 8.60 | $3.02 \times 10^{-6}$ |
| 11.04 | $6.94 \times 10^{-6}$ |
| 14.53 | $1.38 \times 10^{-5}$ |
| 19.40 | $3.83 \times 10^{-5}$ |
| 23.86 | $1.45 \times 10^{-4}$ |
| 24.00 | $1.00 \times 10^{-2}$ |

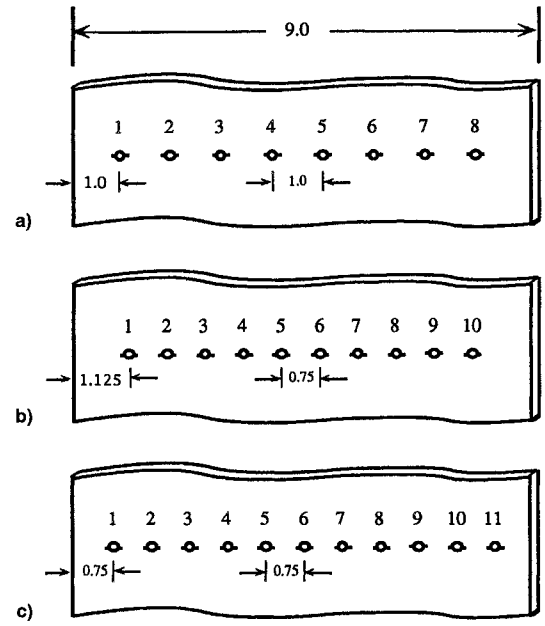


**Fig. 3 Schematic view of hole spacing for various type A MSD test specimens. The nominal hole diameter is 0.16 in. and total specimen width is 9.0 in. Specimens a) MSD02, 03, and 04; b) MSD09; and c) MSD10.**

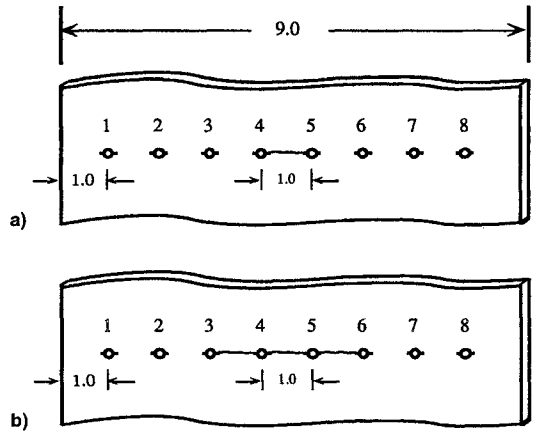


**Fig. 4 Schematic view of hole spacing and crack configurations for various type B MSD specimens. Nominal hole diameter is 0.16 in. and specimen width is 9.0 in. Specimens a) MSD05 and b) MSD06.**

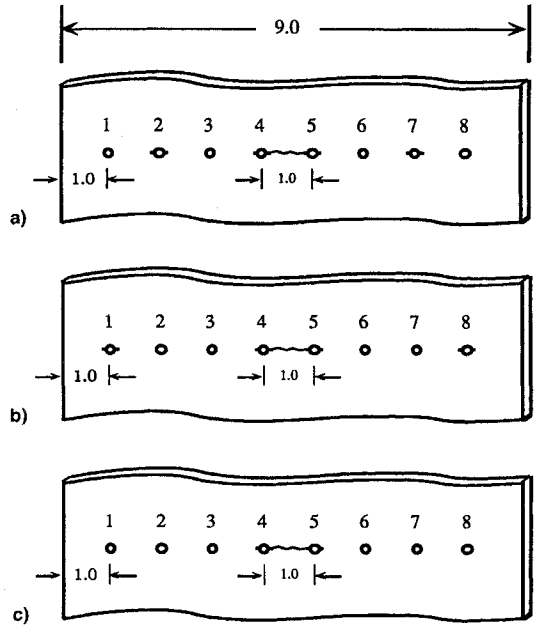


**Fig. 5 Schematic view of hole spacing and crack configuration for various type B MSD specimens. Nominal hole diameter is 0.16 in. and specimen width is 9.0 in. Specimens a) MSD07 with lead crack and MSD cracks at holes 2 and 7, b) MSD08 with lead crack and MSD cracks at holes 1 and 8, and c) MSD11 with lead crack only (no MSD).**

permitted small, uniform cracks to initiate at MSD holes before the central crack grew too large.

The fatigue life of an MSD specimen began once measurable MSD cracks (usually cracks greater than 0.13 mm = 0.005 in. in length as measured from the starter notch edge) had initiated at all holes designed to have MSD. The initial crack lengths were measured using a traveling optical microscope with digital readout, and the specimen was cyclically loaded until complete failure across the midsection occurred. Table 2 lists the effective initial crack lengths for the six type A MSD specimens, and Table 3 lists them for the six type B specimens. The crack length $a_L$ in Tables 2 and 3 is measured from the left side of the hole (including the starter notch), whereas $a_R$ designates the crack length (and notch) from the right side of the hole.

All MSD specimens were loaded parallel to the major axis at a cyclic frequency of 5 Hz. The load amplitude was kept constant, and the $R$ ratio was maintained near 0.01 to match the baseline tests. (Here, $R = \sigma_{min}/\sigma_{max}$, where $\sigma_{max}$ and $\sigma_{min}$ are the maximum and minimum applied remote stresses, respectively.) Table 4 lists the remote stresses applied to each MSD specimen.

All cracks were measured periodically, with the cyclic interval between measurements determined primarily as a function of the fatigue crack growth rate. Initially, longer intervals (such as 5000 cycles) were used during the slow crack growth period. As crack-tips approached each other, or when crack growth became rapid, the measurement intervals were shortened as appropriate to obtain detailed crack growth data.

The MSD tests ended when rapid crack growth and link-up occurred, followed almost immediately by total failure across the midsection of the panel. When failure occurred, the total number of cycles was recorded and the specimen was removed from the testing machine. Prior to discussing the results of the fatigue crack growth tests, however, the numerical analysis for the fatigue life of the MSD specimens will first be discussed.

## Numerical Analysis

A fatigue analysis was developed to predict the initiation and growth of MSD cracks emanating from a row of open fastener holes as remote cyclic loads are applied. The computer algorithm is relatively simple in concept. Given the initial specimen geometry, MSD configuration and loading conditions, the stress intensity factor range $\Delta K$ is computed at each crack tip. The fatigue crack growth rate $da/dN$ is then calculated for each crack using the $da/dN$ vs $\Delta K$ relationship given in Fig. 2. Next, the number of cycles $\Delta N$ to grow the smallest crack a specified amount $\Delta$ is calculated by Eq. (1):

$$\Delta N = \Delta \Big/ \frac{da}{dN} \tag{1}$$

Here, $da/dN$ is the crack growth rate associated with the smallest crack, and the value $\Delta$ employed in Eq. (1) was taken as 0.1% of the length of the smallest crack. Next, the corresponding crack growth increment $\Delta a$ at all other crack tips is calculated from Eq. (2):

$$\Delta a = \Delta N \left(\frac{da}{dN}\right) \tag{2}$$

Now $da/dN$ is the value associated with the particular crack tip of interest. These steps are iterated until the panel fails by one of several criteria. The following subsections describe the stress intensity factor solutions developed for the MSD configurations, the failure criteria employed to specify final life, and the crack initiation concepts used to analyze holes without pre-existent cracks.

While the crack growth model described assumes through-the-thickness MSD cracks, as employed in the tests conducted here, the procedure is readily adapted to consider part-through surface or corner cracks that might be encountered in thicker structural components. In that case, one would replace the through-thickness stress intensity factors described in the next section with the appropriate part-through crack solutions. While the authors have not considered part-through cracks at multiple holes, multiple part-through cracks at a single hole were successfully analyzed by a similar procedure.[10,11]

### Stress Intensity Factors

A compounding method was used to determine stress intensity factors for the MSD specimens. As shown in Figs. 6a and 6b, the through-thickness cracks are treated as either edge cracks, radial hole cracks, or as center cracks (when the radial cracks are large relative to the hole diameters). Linked cracks are considered as either center or edge cracks (the holes are ignored). Once the crack type is designated, an initial solution for $\Delta K$ is calculated and a correction factor is applied to account for the influence of adjacent cracks.

**Table 2 Initial crack lengths for type A MSD specimens (measured from the hole edge and including the starter notch length)**

| Hole no. | Crack tip | Crack length $a$, in. MSD 02 | MSD 03 | MSD 04 | MSD 04b | MSD 09 | MSD 10 |
|---|---|---|---|---|---|---|---|
| 1 | $a_L$ | 0.094 | 0.046 | 0.117 | 0.080 | 0.068 | 0.083 |
| 1 | $a_R$ | 0.128 | 0.046 | 0.103 | 0.107 | 0.088 | 0.092 |
| 2 | $a_L$ | 0.126 | 0.042 | 0.083 | 0.077 | 0.091 | 0.071 |
| 2 | $a_R$ | 0.136 | 0.062 | 0.086 | 0.061 | 0.089 | 0.086 |
| 3 | $a_L$ | 0.149 | 0.066 | 0.065 | 0.077 | 0.142 | 0.079 |
| 3 | $a_R$ | 0.143 | 0.079 | 0.080 | 0.082 | 0.136 | 0.082 |
| 4 | $a_L$ | 0.057 | 0.065 | 0.117 | 0.073 | 0.077 | 0.069 |
| 4 | $a_R$ | 0.061 | 0.083 | 0.134 | 0.076 | 0.060 | 0.077 |
| 5 | $a_L$ | 0.126 | 0.114 | 0.090 | 0.083 | 0.097 | 0.074 |
| 5 | $a_R$ | 0.127 | 0.085 | 0.075 | 0.076 | 0.093 | 0.076 |
| 6 | $a_L$ | 0.095 | 0.067 | 0.102 | 0.091 | 0.103 | 0.061 |
| 6 | $a_R$ | 0.120 | 0.068 | 0.106 | 0.085 | 0.058 | 0.055 |
| 7 | $a_L$ | 0.000 | 0.082 | 0.100 | 0.085 | 0.106 | 0.064 |
| 7 | $a_R$ | 0.029 | 0.079 | 0.100 | 0.095 | 0.082 | 0.089 |
| 8 | $a_L$ | 0.108 | 0.071 | 0.070 | 0.061 | 0.090 | 0.080 |
| 8 | $a_R$ | 0.054 | 0.062 | 0.086 | 0.057 | 0.099 | 0.074 |
| 9 | $a_L$ | — | — | — | — | 0.054 | 0.091 |
| 9 | $a_R$ | — | — | — | — | 0.091 | 0.094 |
| 10 | $a_L$ | — | — | — | — | 0.066 | 0.091 |
| 10 | $a_R$ | — | — | — | — | 0.082 | 0.113 |
| 11 | $a_L$ | — | — | — | — | — | 0.111 |
| 11 | $a_R$ | — | — | — | — | — | 0.086 |
| Average MSD crack | | 0.097 | 0.070 | 0.095 | 0.079 | 0.089 | 0.082 |

**Table 3 Initial crack lengths for type B MSD specimens (measured from the hole edge and including the starter notch length)**

| Hole no. | Crack tip | Crack length $a$, in. MSD 05 | MSD 05b | MSD 06 | MSD 07b | MSD 08 | MSD 11 |
|---|---|---|---|---|---|---|---|
| 1 | $a_L$ | 0.140 | 0.120 | 0.087 | 0.000 | 0.152 | 0.000 |
| 1 | $a_R$ | 0.150 | 0.092 | 0.087 | 0.000 | 0.158 | 0.000 |
| 2 | $a_L$ | 0.104 | 0.064 | 0.104 | 0.066 | 0.000 | 0.000 |
| 2 | $a_R$ | 0.103 | 0.124 | 0.111 | 0.083 | 0.000 | 0.000 |
| 3 | $a_L$ | 0.108 | 0.077 | 0.125 | 0.000 | 0.000 | 0.000 |
| 3 | $a_R$ | 0.069 | 0.097 | 0.421 | 0.000 | 0.000 | 0.000 |
| 4 | $a_L$ | 0.067 | 0.110 | 0.421 | 0.092 | 0.070 | 0.134 |
| 4 | $a_R$ | 0.421 | 0.420 | 0.421 | 0.423 | 0.421 | 0.419 |
| 5 | $a_L$ | 0.421 | 0.420 | 0.421 | 0.423 | 0.421 | 0.419 |
| 5 | $a_R$ | 0.064 | 0.107 | 0.419 | 0.068 | 0.055 | 0.081 |
| 6 | $a_L$ | 0.050 | 0.130 | 0.419 | 0.000 | 0.000 | 0.000 |
| 6 | $a_R$ | 0.053 | 0.157 | 0.115 | 0.000 | 0.000 | 0.000 |
| 7 | $a_L$ | 0.064 | 0.210 | 0.107 | 0.055 | 0.000 | 0.000 |
| 7 | $a_R$ | 0.076 | 0.192 | 0.072 | 0.093 | 0.000 | 0.000 |
| 8 | $a_L$ | 0.000 | 0.190 | 0.130 | 0.000 | 0.104 | 0.000 |
| 8 | $a_R$ | 0.000 | 0.201 | 0.115 | 0.000 | 0.134 | 0.000 |
| 9 | $a_L$ | — | — | — | — | — | — |
| 9 | $a_R$ | — | — | — | — | — | — |
| 10 | $a_L$ | — | — | — | — | — | — |
| 10 | $a_R$ | — | — | — | — | — | — |
| 11 | $a_L$ | — | — | — | — | — | — |
| 11 | $a_R$ | — | — | — | — | — | — |
| Average MSD crack | | 0.076 | 0.138 | 0.102 | 0.074 | 0.137 | 0.000 |

If a crack extends to the edge of the panel as shown in Fig. 6a, then the edge crack solution[12] given in Eqs. (3) and (4) is used to compute the initial $K$:

$$K = \sigma\sqrt{\pi a}\beta_e \tag{3}$$

where

$$\beta_e = 1.12 - 0.231(a/W) + 10.55(a/W)^2 - 21.72(a/W)^3 + 30.39(a/W)^4 \tag{4}$$

In Eqs. (3) and (4) $\sigma$ is the remotely applied stress, $a$ is the edge crack length, and $W$ is the panel width. If the crack does not reach a free edge, the Dowling transition crack length $a_t$ (Ref. 13) given in Eq. (5) is used to determine whether to treat the crack as a radial cracked hole or as a center crack:

$$a_t = \frac{r}{[(1.12 \times K_t)^2 - 1]} \tag{5}$$

Here, $r$ is the hole radius and $K_t$ is the stress concentration factor for the notch geometry. If the crack length is less than

**Table 4 Summary of hole sizes, lead crack lengths, remotely applied stress, and fatigue lives for MSD specimens**

| Specimen ID | Number of holes | Average hole diameter, in. | Hole spacing, in. | Lead crack length, $2a$ | $\sigma_{max}$, ksi | $\sigma_{min}$, ksi | Stress range | Fatigue life cycling |
|---|---|---|---|---|---|---|---|---|
| | | | Type A specimens[a] | | | | | |
| MSD02 | 8 | 0.150 | 1.00 | None | 10.82 | 0.13 | 10.69 | 22,410 |
| MSD03 | 8 | 0.150 | 1.00 | None | 10.82 | 0.13 | 10.69 | 33,310 |
| MSD04 | 8 | 0.158 | 1.00 | None | 12.04 | 0.15 | 11.89 | 20,451 |
| MSD04b | 8 | 0.164 | 1.00 | None | 11.96 | 0.15 | 11.81 | 23,990 |
| MSD09 | 10 | 0.162 | 0.75 | None | 8.64 | 0.11 | 8.53 | 38,871 |
| MSD10 | 11 | 0.162 | 0.75 | None | 8.63 | 0.11 | 8.52 | 36,020 |
| | | | Type B specimens[b] | | | | | |
| MSD05 | 8 | 0.160 | 1.00 | 1.29 | 6.02 | 0.07 | 5.95 | 109,230 |
| MSD05b | 8 | 0.161 | 1.00 | 1.38 | 5.99 | 0.07 | 5.92 | 65,450 |
| MSD06 | 8 | 0.160 | 1.00 | 3.40 | 6.02 | 0.07 | 5.95 | 16,853 |
| MSD07 | 8 | 0.162 | 1.00 | 1.33 | 6.01 | 0.07 | 5.94 | 179,635 |
| MSD08 | 8 | 0.162 | 1.00 | 1.29 | 6.00 | 0.07 | 5.93 | 205,930 |
| MSD11 | 8 | 0.166 | 1.00 | 1.34 | 6.00 | 0.07 | 5.93 | 215,680 |

[a]Those with no lead cracks. [b]Those with central lead cracks.

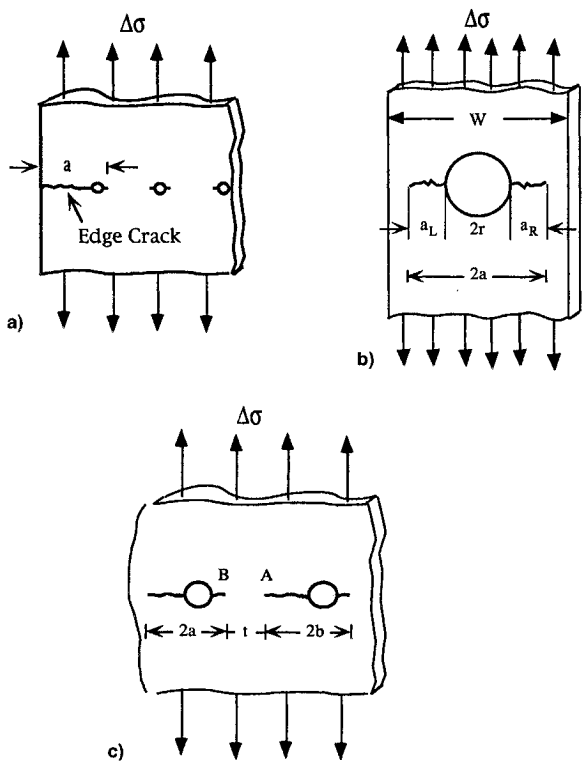


**Fig. 6 Schematic representation of various crack configurations modeled in MSD crack analysis: a) edge crack configuration, b) radially cracked hole configuration, and c) adjacent hole cracks prior to coalescence.**

$a_t$, Eq. (6) is used for $K$, and if it is larger than this size, the well-known center cracked $K$ solution given by Eq. (7) is employed.[12]

If $a < a_t$:

$$K = \sigma\sqrt{\pi a}\beta_h \tag{6}$$

Here, crack length $a$ is measured from the edge of the hole as shown in Fig. 6b for crack lengths $a_L$ and $a_R$. The dimensionless factor $\beta_H$ for a radially cracked hole[14] with radius $r$, is given by Eq. (8):

$$\beta_H = \left(\frac{F_1}{F_2 + a/r} + F_3\right) \tag{7}$$

For holes with cracks emanating from both sides, $F_1 = 0.6865$, $F_2 = 0.2772$, and $F_3 = 0.9439$. For holes with only one side cracked, $F_1 = 0.8733$, $F_2 = 0.3245$, and $F_3 = 0.6762$.

If $a \geq a_t$, the cracked holes are treated as center cracks with Eq. (8):

$$K = \sigma\sqrt{\pi a}\beta_w \tag{8}$$

Here, $\beta_w$ is the stress intensity factor coefficient[12] for a center crack of length $2a$ in a plate of width $W$ [the hole diameter is included in the total crack length $2a$ given by Eq. (9)]:

$$\beta_w = \sqrt{\sec(\pi a/W)} \tag{9}$$

Once the initial cyclic $K$ is computed, a crack interaction factor is applied to account for the presence of adjacent cracks. The crack interaction factor was based on the Kamei and Yokobori $K$ solution[15] for two interacting cracks shown in Fig. 6c. For the configuration shown in Fig. 6c, this solution gives the following stress intensity factors $K_A$ at crack tip $A$ and $K_B$ at tip $B$. (This solution ignores the influence of the hole, assuming the crack lengths are large relative to the hole radius.)

$$K_A = \sigma\sqrt{\pi b}\sqrt{1 + \frac{2a}{t}}\left\{1 - \left(1 + \frac{t}{2b}\right)\left[\frac{K(k) - E(k)}{K(k)}\right]\right\} \tag{10}$$

$$K_B = \sigma\sqrt{\pi a}\sqrt{1 + \frac{2b}{t}}\left\{1 - \left(1 + \frac{t}{2a}\right)\left[\frac{K(k) - E(k)}{K(k)}\right]\right\} \tag{11}$$

Here, $K(k)$ and $E(k)$ are the complete elliptic integrals of the first and second kind, respectively, $a$ and $b$ are the crack lengths, and $t$ is the crack separation distance shown in Fig. 6c. The kernel $k$ for the elliptic integrals is given by Eq. (12):

$$k = 2\sqrt{ab/\langle(2a + t)(2b + t)\rangle} \tag{12}$$

It was later found experimentally that the Kamei and Yokobori interaction factor consistently underestimated the crack interaction in the MSD specimens considered here. To match the measured crack growth lives, the Kamei and Yokobori interaction factor was empirically modified by replacing the crack tip spacing $t$ in Eqs. (10) and (11) with an effective crack

tip spacing $t_{eff} = 0.4t$. When $t_{eff}$ was used in place of $t$ to compute the Kamei and Yokobori interaction factors, close correlation was achieved between the predicted and experimental lives for all of the different types of interacting cracks in the MSD specimens. Thus, $t_{eff}$ is used to calculate interaction factors in all crack growth and fatigue life predictions made in this analysis.

There are several possible reasons why the original Kamei and Yokobori crack tip interaction factor needed to be empirically modified for the present experiments. The basic accuracy of the linear elastic Yokobori and Kamei stress intensity factor solutions may be in question, and they could, perhaps, be studied by other numerical analyses of the crack interaction problem. Another obvious explanation may be because of the violation of linear elastic fracture mechanics (LEFM) assumptions in the large crack tip plastic zones formed by the interacting fatigue cracks in the ductile 2024-T3 test material. Such plasticity effects would certainly be dependent on the type of material and specimen thickness. A detailed analysis of the crack interaction problem was, however, beyond the scope of this article. While the empirical $0.4t$ effective crack spacing correction worked well for the current experiments, it should receive further evaluation before being applied to other materials or specimen thicknesses.

### Failure Criteria

Once MSD has formed in a panel, the individual cracks continue to grow until they link-up or until the panel fails. Different criteria may be chosen during the analysis to determine when failure will occur as described in Refs. 6 and 7. For the current analysis, the net section yield method was used to predict failure of type A specimens, and a ligament yield criterion proposed by Swift[3] was used for predicting failure in type B specimens. The net section yield method assumed the panel fails when the net section stress exceeds the tensile yield stress found from the stress–strain tests. Swift's ligament yield RS criterion states that a large lead crack will cause panel failure when its crack tip plastic zone touches that of an adjacent flaw (MSD crack). Further details of these criteria and separate RS tests conducted to verify them for the types of panels studied here, are described in Refs. 6 and 7.

### Crack Formation Concepts

The type B specimens shown in Fig. 5 contained some holes that were not initially cracked. Although these holes act as crack arresters when a crack grows into them from a neighboring hole, eventually a crack develops on the opposite side and begins to propagate outward. Thus, crack formation calculations are also required to compute the total fatigue lives for these specimens. There are two basic notch geometries where cracks may initiate in the type B specimens: 1) geometry I: a circular hole with no cracks at either side and 2) geometry II: a circular hole that has been penetrated at one side by a propagating crack.

The number of cycles required to initiate new cracks at these configurations were estimated from the following well-known strain-life equations.[16]

### Cyclic Strain-Life

$$\Delta\varepsilon/2 = [(\sigma_{f'} - \sigma_0)/E](2N_f)^b + \varepsilon_{f'}(2N_f)^c \quad (13)$$

Here, $\sigma_{f'}$ is the fatigue strength coefficient, $\sigma_0$ is the mean remotely applied stress, $2N_f$ is the number of reversals to crack initiation (two reversals = one cycle), $\Delta\varepsilon$ is the strain range at the notch root, $\varepsilon_{f'}$ is the fatigue ductility coefficient, $b$ is the fatigue strength exponent, and $c$ is the fatigue ductility exponent.

### Cyclic Stress–Strain Curve

$$\Delta\varepsilon/2 = (\Delta\sigma/2E) + (\Delta\sigma/2K')^{1/n'} \quad (14)$$

In Eq. (14) $K'$ is the cyclic strength coefficient for the material, $n'$ is the cyclic strain hardening exponent, $E$ is Young's modulus, and $\Delta\sigma$ is the stress range at the notch root.

### Neuber's Rule

$$(K_f\Delta S_{net})^2/E = (\Delta\sigma)(\Delta\varepsilon) \quad (15)$$

In Eq. (15) $\Delta S_{net}$ is the net section stress range (the remote load divided by the net cross-sectional area at the notch) and $K_f$ is the fatigue concentration factor.

The material constants $\sigma_{f'}$, $\varepsilon_{f'}$, $b$, $K'$, and $n'$ were taken from published values given in Ref. 16 for 2024-T3 aluminum, and the elastic modulus $E$ was obtained from the stress–strain tests described earlier. The fatigue concentration factor $K_f$ can be related to the elastic stress concentration factor $K_t$ for the notch from the following expression[16]:

$$K_f = 1 + [(K_t - 1)q] \quad (16)$$

The fatigue notch sensitivity factor $q$ can be approximated by the following empirically derived relationship[16]:

$$q = 1/(1 + \sqrt{\rho/r}) \quad (17)$$

Here, $\rho$ is a material constant called the Neuber equivalent grain half-length, and $r$ is the notch root radius. The value for $\rho$ was again taken from data given by Bannantine et al.[16] for 2024-T3 aluminum.

Equations (13–17) are solved simultaneously for the initiation life $2N_f$ (measured in reversals) using an iterative technique. Because the damage during each cycle varies, as the net section stress increases because of crack growth from adjacent holes, a method must be chosen to determine when the accumulated damage is sufficient to cause crack initiation. Miner's linear cumulative damage rule[16] was used for this purpose, and assumes a crack has formed when

$$\sum (2n_i/2N_i) \geq 1 \quad (18)$$

In Eq. (18), $2n_i$ are the number of applied reversals at the given load, and $2N_i$ is the fatigue life that would occur if only the $2n_i$ loads were applied.

Because the damage for each cycle is computed using current crack lengths and configurations, the use of Miner's rule accounts for changes in the net section stress as the cracks at other holes or notches propagate during the fatigue life of a panel. When the Miner's rule sum reaches a value of 1, the initiation life is considered complete, and crack propagation begins at the location of interest. The initial crack size assumed

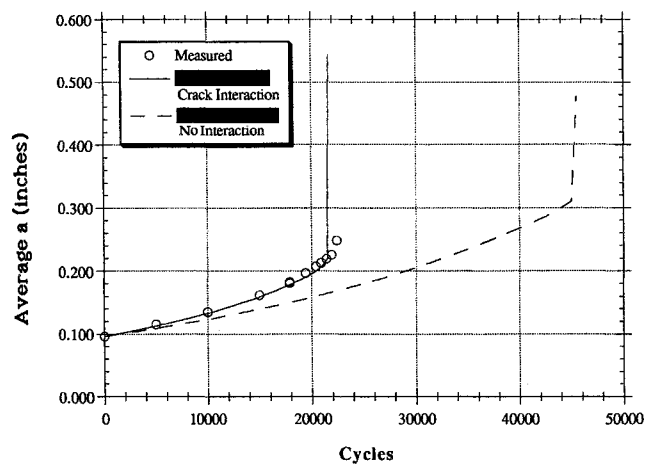


**Fig. 7 Average crack length $a$ as a function of elapsed cycles for specimen MSD02.**

after the initiation process is complete was based on Dowling's transition crack length $a_t$ (Ref. 13) given previously in Eq. (5).

In summary, when a type B panel with uncracked holes is analyzed, strain-life concepts along with Miner's rule are used to estimate crack initiation at the holes. When this occurs, a crack equal to the Dowling transition crack length $a_t$ is placed at the location of interest, and then the algorithm continues to propagate that crack, as it does for all other cracks, until link-up or panel failure occurs.

## Discussion of Results

This section describes typical fatigue crack growth results from the MSD fatigue tests, and compares the measured data with calculations obtained by the numerical analysis described in the preceding section. Additional details and results are given in Ref. 7. In that report, crack growth curves for all of the experiments and predictions are given in the following formats.

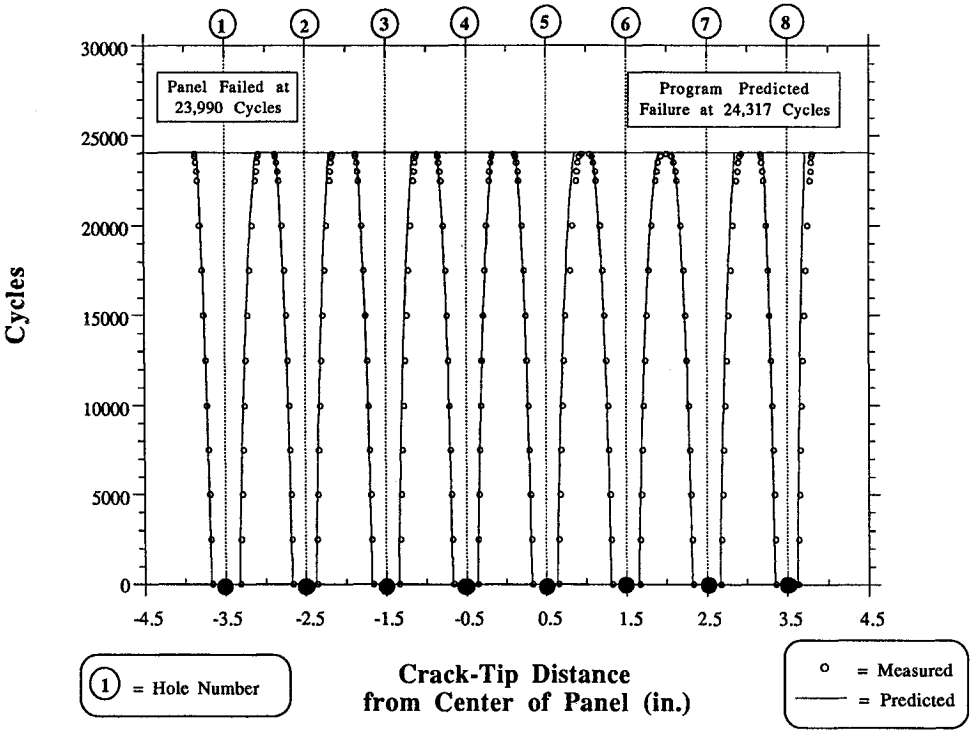


**Fig. 8 Fatigue crack propagation diagram for type A specimen MSD04b.**

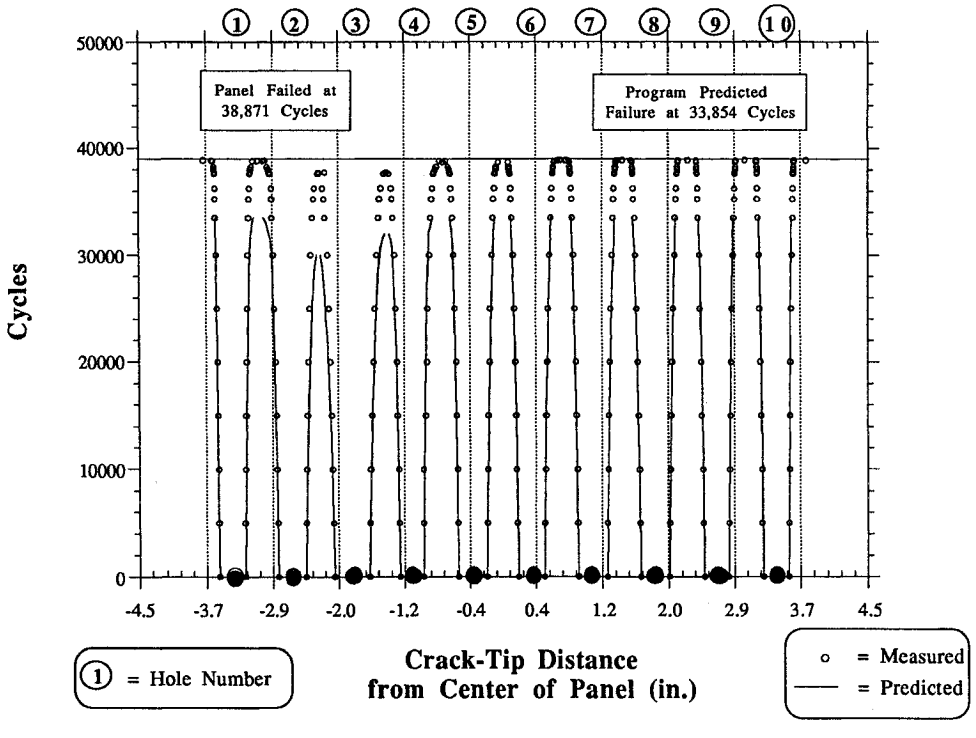


**Fig. 9 Fatigue crack propagation diagram for type A specimen MSD09.**

1) *Average crack length curves*: The average crack length $a$ for all MSD cracks in a typical panel is plotted as a function of elapsed cycles as shown in Fig. 7. The actual crack length measurements are compared with two predictions shown for each test: one that includes crack interaction effects and one that omits them. The average crack length predictions demonstrate the program's ability to analyze the fatigue lives of the panels, and clearly show the effects of crack interaction on crack growth rates.

2) *Crack propagation diagrams*: The position of each crack tip is also plotted as a function of elapsed cycles as shown in Fig. 8. The crack tip locations are plotted to scale, with large black circles along the $x$ axis representing the location and size of each hole in the test panel. Hole identification numbers are also given along the top of each diagram. Both predicted and measured crack tip positions are plotted, with the experimental data represented by open circles and the predictions shown by solid lines. These diagrams show the individual crack growth

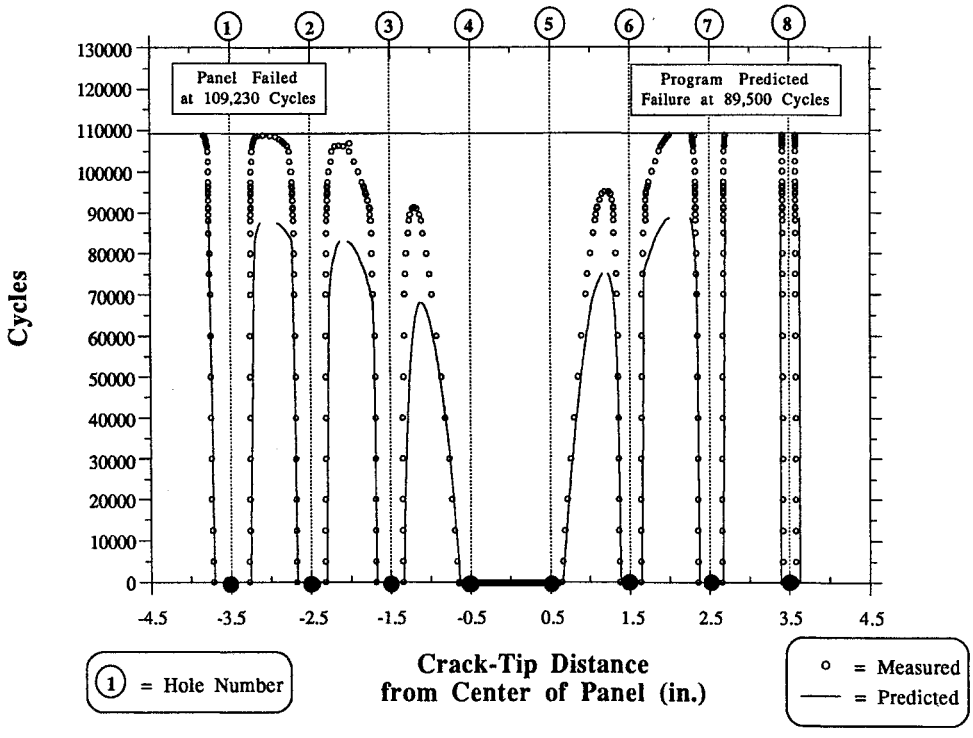


**Fig. 10 Fatigue crack propagation diagram for type B specimen MSD05.**

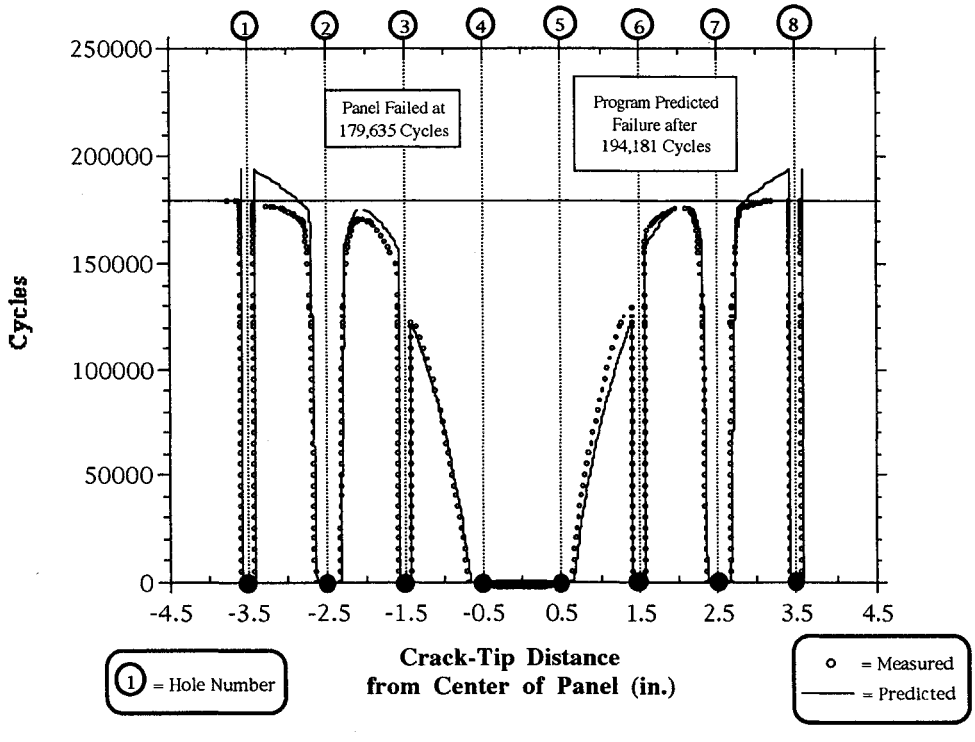


**Fig. 11 Fatigue crack propagation diagram for type B specimen MSD07. Note that holes 1, 3, 6, and 8 were not initially cracked.**

curves and graphically demonstrate the effects cracks have on each other. They also show when link-up occurred between cracks, and when rapid growth rates began for individual cracks. Since these latter curves yield more information than the average crack growth curves, this format will be used for the remainder of this article.

Figures 8 and 9 compare measured and predicted fatigue crack growth curves for two of the type A specimens (those with small MSD cracks at each open hole). These specimens were similar in design except for a difference in the number of holes and hole spacing. Note that the numerical algorithm tracks individual cracks quite well and gives a good estimate for the total fatigue life.

Figures 10–13 show typical results for the type B specimens, which contained large lead cracks along with various numbers of small MSD cracks at the other holes. Figure 10 presents a lead crack case where all of the holes contained MSD, and again, the analysis predicts growth of individual cracks and total fatigue life quite well. Figures 11 and 12 are lead crack cases where only two holes contained MSD (hole

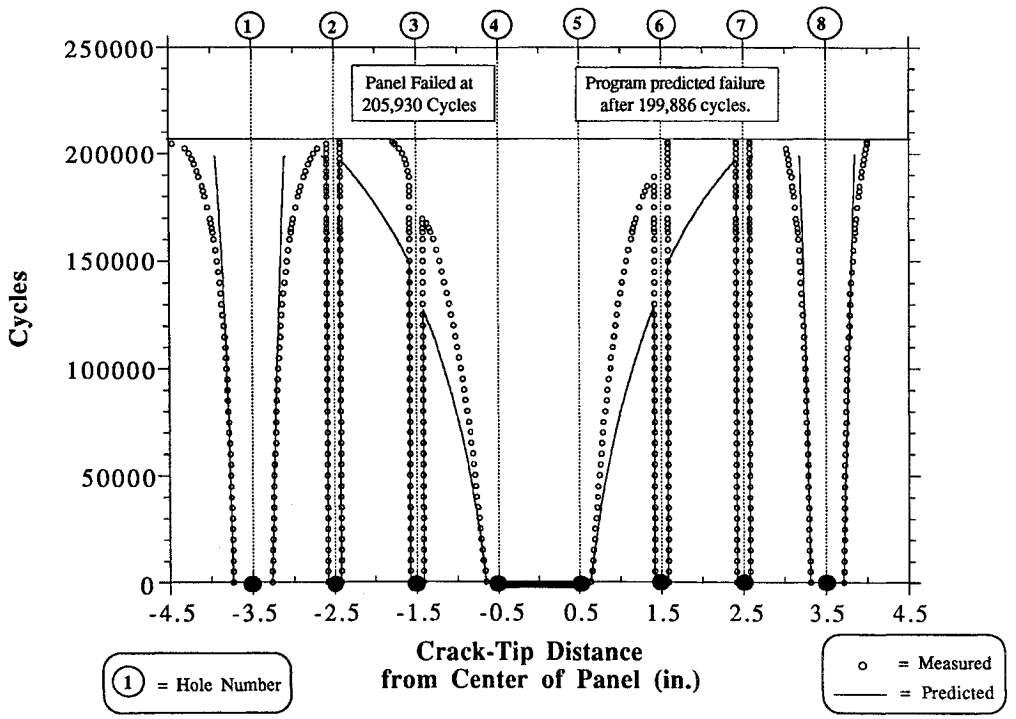


**Fig. 12 Fatigue crack propagation diagram for type B specimen MSD08. Note that holes 2, 3, 6, and 7 were not cracked initially.**

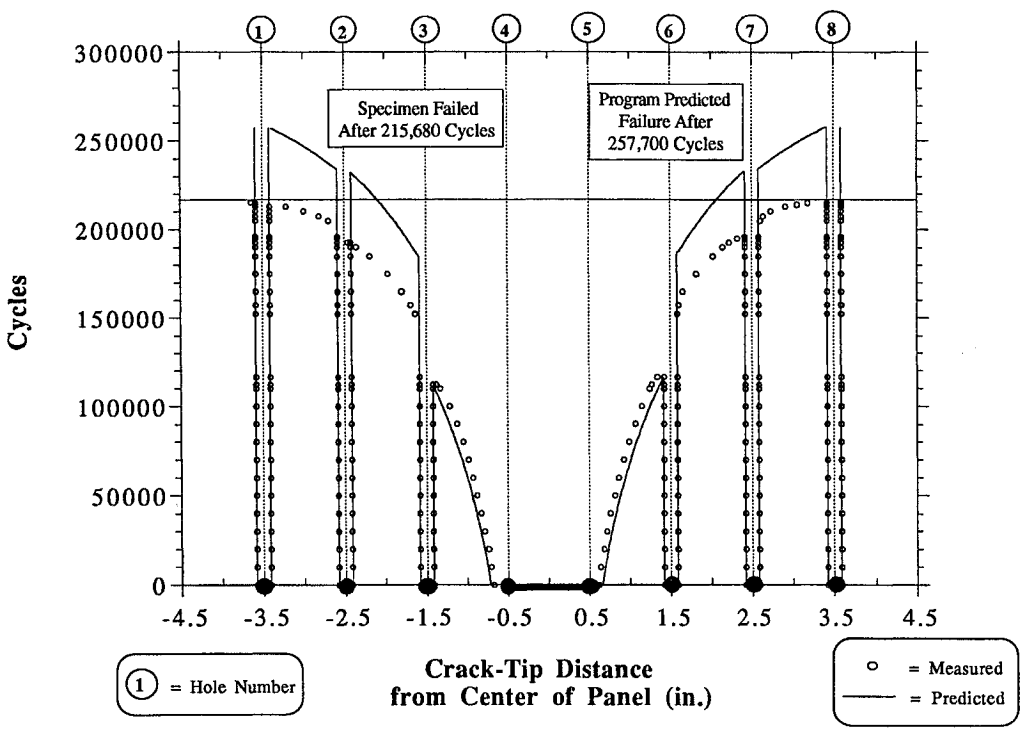


**Fig. 13 Fatigue crack propagation diagram for type B specimen MSD11. Note that this specimen did not contain initial MSD cracks.**

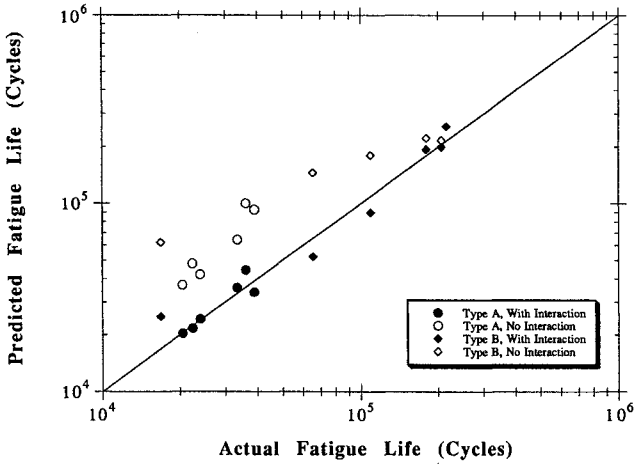


**Fig. 14 Summary comparison of predicted and measured fatigue lives for all MSD specimens.**

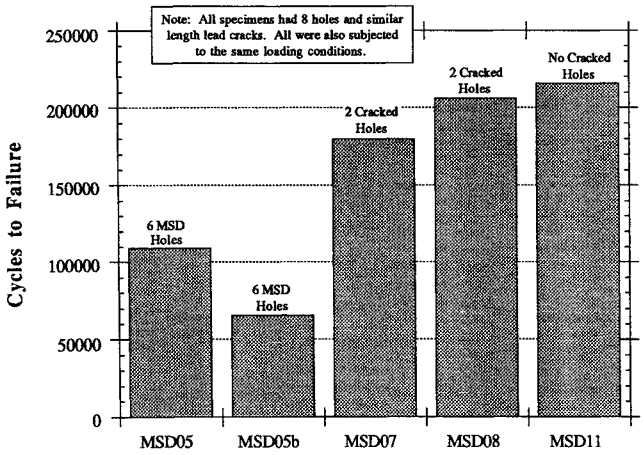


**Fig. 15 Comparison of measured fatigue lives for similar type B specimens showing reduction in fatigue life caused by degree of MSD in holes adjacent to lead crack.**

numbers 2 and 7 in Fig. 11, and holes 1 and 8 in Fig. 12). Figure 13 presents the one test without MSD (only a lead crack was present), and provides a convenient reference with which to compare the effect of MSD. In Figs. 11–13, the crack initiation calculations described previously were employed to restart cracking once a lead crack grew into an uncracked hole. Note that, in general, the strain-life approach to crack initiation gives a good estimate of the life required for cracking to resume at the unflawed side of a hole.

The measured and predicted fatigue lives for all 12 specimens are compared in Fig. 14 and are recorded in Figs. 8–13. The case A specimens (MSD cracking only) are represented by circles in Fig. 14, and the case B cases (lead cracks with full or partial MSD at the remaining holes) are given by diamonds. The solid symbols represent calculations that employed the modified Kamei and Yokobori[13] crack tip interaction factor in the stress intensity factor analysis, while the open symbols represent calculations that ignored crack tip interaction. Note that the crack tip interaction calculations agree well with the test results for all 12 cases examined, including both the complete MSD cases (type A) as well as the lead crack plus full or partial MSD specimens (type B). Ignoring crack tip interaction (open symbols), however, yields an unconservative calculation for total specimen life in both cases.

Finally, Fig. 15 shows the degree to which MSD can reduce the fatigue life for specimens that contain lead cracks (type B). Here five specimens with similar lead crack sizes ($2a$ = 3.3 cm = 1.3 in.) were subjected to the same cyclic stress ($\sigma_{max}$ = 41 MPa = 6 ksi). Specimen MSD11 only contained a lead crack, with the remaining holes initially uncracked, and as expected gave the longest fatigue life. The remaining specimens had full or partial MSD cracks at adjacent holes (average length $a$ = 2.5 mm = 0.1 in.). Specimens MSD07 and MSD08 each contained pairs of precracked holes remote from the lead crack. As shown in Figs. 11 and 12, these MSD holes were separated by at least one uncracked hole between the lead crack and the MSD location. The lives for these specimens were reduced, but not substantially in comparison to the specimen without multisite damage (MSD11). The other two tests (MSD05 and MSD05b) contained initial MSD at all holes, and have substantially shorter lives than the specimen without MSD. Thus, extensive MSD can significantly lower fatigue life, and the effect is the greatest when adjacent holes are cracked.

Finally, it should be noted that this article has employed linear elastic fracture mechanics concepts to analyze MSD panels subjected to constant amplitude loading. In this regard, it is assumed that crack tip plasticity is small, and fatigue crack growth is controlled by the cyclic stress intensity factor as shown in Fig. 2. While LEFM conditions are certainly violated when the crack tips approach each other, resulting in large plastic zones prior to crack coalescence, this occurs late in life, when the cracks are growing rapidly, and has a relatively minor effect on total life. (Various techniques for analyzing the large scale plasticity that occurs at fracture are discussed in Ref. 7.) Another aspect of crack tip plasticity that could be important in structural applications deals with variable amplitude loading. If, for example, peak tensile overloads were applied, it is possible to obtain a delay in crack growth. While many numerical models have been developed to analyze this crack retardation phenomenon, it is not known how crack retardation would be influenced by the presence of adjacent (MSD) crack tips. Since the current work was restricted to constant amplitude loading, variable amplitude considerations are left to future research.

## Summary and Conclusions

An experimental and numerical study has been conducted on panels that contain a row of open holes subjected to various degrees of multisite cracking. The following conclusions can be drawn from the results and discussions of this investigation. (Additional conclusions regarding the RS of MSD panels are given in Refs. 6 and 7.)

1) The interaction of cracks significantly increases the rate of crack growth and reduces the overall fatigue lives of panels with extensive MSD, even when the MSD cracks are initially small in length (approximately 1.2–2.5 mm = 0.05–0.10 in.).

2) The simplifying assumptions described here for the deterministic MSD analysis produce good estimates for crack interaction, crack propagation, and the overall fatigue lives for unstiffened, flat panels with MSD subjected to constant amplitude cyclic loading.

3) The strain-life analysis using Neuber's and Miner's rules provides a good estimate of the initiation time required after a crack has arrested at a hole in a panel with MSD subjected to constant amplitude cyclic loading.

4) The Kamei and Yokobori $\Delta K$ solution for two coalescing cracks[13] underestimates the effect of crack interaction in the MSD fatigue testing of the type conducted in this research. The empirically modified crack interaction correction factor used in this analysis produces more accurate and acceptable results for all configurations tested.

## Acknowledgments

The first author, Commander E. J. Moukawsher, died during the review process after this article was submitted to the *Journal of Aircraft*. He is sorely missed by his friends and colleagues. Portions of this research were also sponsored by Air Force Office of Scientific Research Grant F49620-93-1-0377. The authors wish to thank the U.S. Coast Guard for providing

the test materials and for supporting the graduate studies of E. J. Moukawsher and M. Neussl at Purdue University. The authors especially thank T. Swift of the Federal Aviation Administration for suggesting the ligament yield failure criterion and for his encouragement and advice during the course of the research.

## References

[1]Partl, O., and Schijve, J., "Multiple-Site-Damage in 2024-T3 Alloy Sheet," *International Journal of Fatigue*, Vol. 15, No. 4, 1992, pp. 293–299.

[2]Dawicki, D. S., and Newman, J. C., Jr., "Analysis and Prediction of Multiple-Site Damage (MSD) Fatigue Crack Growth," NASA TP 3231, Aug. 1992.

[3]Swift, T., "Effect of MSD on Residual Strength," Symposium on Multiple Site Damage (MSD) in Aging Aircraft, Warner Robins Air Logistics Center, Robins AFB, GA, Feb. 1992.

[4]Mar, J. W., "Structural Integrity of Aging Airplanes: A Perspective," *Structural Integrity of Aging Airplanes*, edited by S. N. Atluri, S. G. Sampath, and P. Tong, Springer–Verlag, Berlin, 1991.

[5]Hendricks, W. R., "The Aloha Airlines Accident—A New Era for Aging Aircraft," *Structural Integrity of Aging Airplanes*, edited by S. N. Atluri, S. G. Sampath, and P. Tong, Springer–Verlag, Berlin, 1991.

[6]Moukawsher, E. J., Heinimann, M. B., and Grandt, A. F., Jr., "Residual Strength of Panels with Multiple Site Damage," *Journal of Aircraft*, Vol. 33, No. 5, 1996, pp. 1014–1021.

[7]Moukawsher, E. J., "Fatigue Life and Residual Strength of Panels with Multiple Site Damage," M.S. Thesis, School of Aeronautics and Astronautics, Purdue Univ., West Lafayette, IN, May 1993.

[8]"Test Methods of Tension Testing of Metallic Materials," American Society for Testing and Materials, Specification E8-89, July 1991.

[9]"Standard Test Method for Constant-Load-Amplitude Fatigue Crack Growth Rates Above $10^{-8}$ m/Cycle," American Society for Testing and Materials Specification E647-91, June 1991.

[10]McComb, T. H., Pope, J. E., and Grandt, A. F., Jr., "Growth and Coalescence of Multiple Fatigue Cracks in Polycarbonate Test Specimens," *Engineering Fracture Mechanics*, Vol. 24, No. 4, 1986, pp. 601–608.

[11]Grandt, A. F., Jr., Thakker, A. B., and Tritsch, D. E., "An Experimental and Numerical Investigation of the Growth and Coalescence of Multiple Fatigue Cracks at Notches," *Fracture Mechanics: Seventeenth Volume, ASTM STP 905*, American Society for Testing and Materials, Philadelphia, PA, 1986, pp. 239–252.

[12]Rooke, D. P., and Cartwright, D. J., "Compendium of Stress Intensity Factors," *Her Majesty's Stationery Office*, London, 1976.

[13]Dowling, N. E., "Notched Member Fatigue Life Predictions Combining Initiation and Propagation," *Fatigue of Engineering Materials and Structures*, Vol. 2, No. 2, 1979, pp. 129–138.

[14]Grandt, A. F., Jr., "Stress Intensity Factors for Some Thru-Cracked Fastener Holes," *International Journal of Fracture*, Vol. 11, No. 2, 1975, pp. 283–294.

[15]Kamei, A., and Yokobori, T., "Two Collinear Asymmetrical Elastic Cracks," *Report of the Research Institute for Strength and Fracture of Materials*, Tohoku University, Vol. 10, Secs. 1–4, Dec. 1974, pp. 41, 42.

[16]Bannantine, J. A., Comer, J. J., and Handrock, J. L., *Fundamentals of Metal Fatigue Analysis*, Prentice–Hall, Englewood Cliffs, NJ, 1990.